

Dome-shaped magnetic order competing with high-temperature superconductivity at high pressures in FeSe

J. P. Sun,^{1,*} K. Matsuura,^{2,*} G. Z. Ye,^{1,3,*} Y. Mizukami,² M. Shimozawa,⁴
 K. Matsubayashi,⁵ M. Yamashita,⁴ T. Watashige,⁶ S. Kasahara,⁶ Y. Matsuda,⁶
 J.-Q. Yan,^{7,8,†} B. C. Sales,⁷ Y. Uwatoko,⁴ J.-G. Cheng,^{1,‡} and T. Shibauchi^{2,§}

¹*Beijing National Laboratory for Condensed Matter Physics and Institute of Physics,
 Chinese Academy of Sciences, Beijing 100190, China*

²*Department of Advanced Materials Science,
 University of Tokyo, Kashiwa, Chiba 277-8561, Japan*

³*School of Physical Science and Technology,
 Yunnan University, Kunming 650091, China*

⁴*Institute for Solid State Physics, The University of Tokyo, Kashiwa, Chiba 277-8581, Japan*

⁵*Department of Engineering Science,
 The University of Electro-Communications, Chofu, Tokyo 182-8585, Japan*

⁶*Department of Physics, Kyoto University, Sakyo-ku, Kyoto 606-8502, Japan*

⁷*Materials Science and Technology Division,
 Oak Ridge National Laboratory, Oak Ridge, Tennessee 37831, USA*

⁸*Department of Materials Science and Engineering,
 University of Tennessee, Knoxville, Tennessee 37996, USA*

(Dated: December 23, 2015)

* These authors contributed equally to this work.

† Email: jqyan@utk.edu

‡ Email: jgcheng@iphy.ac.cn

§ Email: shibauchi@k.u-tokyo.ac.jp

The coexistence and competition between superconductivity and electronic orders, such as spin or charge density waves, have been a central issue in high transition-temperature (T_c) superconductors [1–3]. Unlike other iron-based superconductors, FeSe exhibits nematic ordering without magnetism [4–6] whose relationship with its superconductivity remains unclear. More importantly, a pressure-induced fourfold increase of T_c has been reported [7, 8], which poses a profound mystery. Here we report high-pressure magnetotransport measurements in FeSe up to ~ 9 GPa, which uncover a hidden magnetic dome superseding the nematic order. Above ~ 6 GPa the sudden enhancement of superconductivity ($T_c \leq 38.3$ K) accompanies a suppression of magnetic order, demonstrating their competing nature with very similar energy scales. Above the magnetic dome we find anomalous transport properties suggesting a possible pseudogap formation, whereas linear-in-temperature resistivity is observed above the high- T_c phase. The obtained phase diagram highlights unique features among iron-based superconductors, but bears some resemblance to that of high- T_c cuprates.

In most iron-based superconductors, superconductivity emerges on the verge of a long-range antiferromagnetically ordered state [3], which is a common feature to many unconventional superconductors including the cuprates and heavy-fermion materials. It has been shown that the antiferromagnetic order in the iron-pnictide materials accompanies or follows the tetragonal-to-orthorhombic structural transition at T_s . In striking contrast to this, the structurally simplest FeSe exhibits a high $T_s \approx 90$ K but no magnetic order appears at lower temperatures [4–6], and still its ground state is an unconventional superconducting state with $T_c \approx 9$ K [9, 10]. This material is also intriguing in that in the form of one-unit-cell-thick films a very high T_c (up to 109 K) has been reported recently [11–13], which is likely associated with a carrier doping effect [14, 15] from the substrate. In bulk FeSe, a significant electronic anisotropy is found below T_s in the nonmagnetic orthorhombic phase, which is often called a nematic state [9, 10]. In the nematic phase, very small Fermi surfaces with strong deviations from the first-principles calculations have been observed [10, 16], and the occurrence of superconductivity with such small Fermi energies is quite unusual, implying that the system is deep in the crossover regime between the weak-coupling Bardeen-Cooper-Schrieffer (BCS) and strong-coupling Bose-Einstein-condensate (BEC) limits [10].

In addition to these distinct electronic characteristics of FeSe, remarkable properties have been reported under high pressure [7, 8, 17–21]. First of all, the powder sample study has shown that the relatively low $T_c \approx 9$ K at ambient pressure can be enhanced by more than fourfold to ~ 37 K under ~ 8 GPa, pushing it into the class of high- T_c superconductors [7]. More recent studies on single crystals under better hydrostatic pressure conditions revealed a complex temperature-pressure (T - P) phase diagram featured by a suppression of T_s around 2 GPa, a sudden development of static magnetic order above ~ 1 GPa [17], and an enhancement of T_c in a three-plateau process [8], i.e. $T_c \sim 10(2)$ K for 0-2 GPa, $T_c \sim 20(5)$ K for 3-5 GPa, and $T_c \sim 35(5)$ K for 6-8 GPa. The first jump of T_c from ~ 10 K to ~ 20 K seems to coincide with the suppression of the nonmagnetic nematic state and the development of the long-range magnetic order at T_m evidenced by μ SR measurements [17]. The observation that both T_c and T_m increase with pressure in the pressure range 1-2.5 GPa has been taken as evidence for the cooperative promotion of superconductivity by the static magnetic order. Such a scenario, however, does not fit into the general scope of iron-based superconductors, in which the optimal superconductivity is realized when the long-range magnetic order is close to collapse [3, 22]. This issue remains unclear unless the fate of magnetic order at T_m under higher pressures is sorted out. Due to the technical limitations of probing small-moment magnetic order above 3 GPa, this task only becomes possible very recently when a clear signature at T_m is visible in the resistivity [18–20] of high-quality FeSe single crystals [23].

Here, by performing the high-pressure resistivity $\rho(T)$ measurements up to ~ 9 GPa on high-quality single crystals, we construct for bulk FeSe the most comprehensive T - P phase diagram mapping out the explicit evolutions with pressure of T_s , T_c , and T_m . As shown in Fig. 1, we uncover a previously unknown dome-shaped $T_m(P)$, having two end points situated on the boundaries separating the three plateaus of $T_c(P)$. Our results thus provide compelling evidence linking intimately the sudden enhancement of T_c to 38 K to the suppression of long-range magnetic order. This highlights a competing nature between magnetic order and high- T_c superconductivity in the phase diagram of FeSe, which is a key material among the iron-based superconductors.

The orthorhombic-tetragonal structure transition at $T_s \approx 90$ K for bulk FeSe is manifested as a slight upturn in resistivity, which can be taken as a signature to track down the evolution of T_s with pressure. Our resistivity $\rho(T)$ data measured with a self-clamped

piston-cylinder cell (PCC) up to ~ 1.9 GPa are shown in Fig. 2a. As can be seen, T_s is suppressed progressively to below 50 K at ~ 1.5 GPa, above which the anomaly at T_s becomes poorly defined. Meanwhile, a second anomaly manifested as a more profound upturn in $\rho(T)$ emerges at $T_m \sim 20$ K and moves up steadily with pressure. In light of the recent high-pressure μ SR study [17], this anomaly at T_m corresponds to the development of long-range magnetic order. T_s and T_m seem to cross around ~ 2 GPa. In this pressure range, the superconducting transition temperature T_c (defined as the zero-resistivity temperature) first increases and then decreases slightly before rising again. This features a small dome-shaped $T_c(P)$ peaked at ~ 1.2 GPa (Fig. 1), which roughly coincides with the pressure where the long-range magnetic order at T_m starts to emerge. These results in this relatively low pressure range are in general consistent with those reported previously [18–20].

To further track down the evolution of T_m , we turn to $\rho(T)$ measurements in the cubic anvil cells (CACs) that can maintain a quite good hydrostaticity up to ~ 9 GPa [24, 25]. Figures 2b and 2c display the $\rho(T)$ data measured in the self-clamped CAC and the constant-loading CAC, respectively (see Methods for experimental details). In line with the results of PCC in Fig. 2a, the sudden upturn is clearly visible at T_m in both measurements in a pressure range up to ~ 2.5 GPa (Figs. 2b, 2c, 3a, 3b), above which the upturn anomaly disappears and instead a kink appears in $\rho(T)$ followed by a gradual drop before reaching the superconducting transition (Figs. 2b, 2c, 3c, 3d). Our self-clamped CAC enables us to measure $\rho(T)$ under different magnetic fields [24, 25], which clearly resolves that this anomaly is of the same origin as the magnetic order at lower pressures. As seen in Fig. 4b, upon the application of magnetic fields the resistivity kink at 2.8 GPa restores to the upturn anomaly and this anomaly shows little field dependence as that observed at 1.8 GPa (Fig. 4a). Upon further increasing pressures, T_m moves up gradually and reaches about 45 K at 4.8 GPa, where the resistivity kink becomes sharper (Fig. 2b). In striking contrast with the progressive enhancement of T_m in this pressure range of 2–5 GPa, T_c remains nearly unchanged at the second plateau of ~ 20 K.

The situation changes dramatically when further increasing pressure above ~ 5 GPa. As shown in Figs. 2b and 3d, $\rho(T)$ at 5.8 GPa exhibits an abrupt drop at 38.5 K before reaching zero resistivity at $T_c = 27.5$ K, and then at 6.3 GPa the abrupt drop develops into a very sharp superconducting transition at $T_c = 38.3$ K with a transition width of only 0.4 K (Figs. 2b and 3e). Thus, T_c is nearly doubled from ~ 20 K at 4.8 GPa to 38.3 K at 6.3 GPa,

and the abrupt drop at 38.5 K under 5.8 GPa corresponds to the onset of superconductivity rather than the magnetic order, which is supported by the large change under magnetic fields (Fig. 4d). Then, what is the fate of T_m ? A closer inspection of the $\rho(T)$ data at 5.8 GPa reveals an inflection point at the temperature slightly above the abrupt drop. This feature can be well resolved from the temperature derivative of resistivity $d\rho/dT$ in Fig. 3d. Here the small peak centred at 41 K corresponds to T_m , which is confirmed by the field independence (Fig. 4d). At 6.3 GPa, such a magnetic anomaly is absent in the $d\rho/dT(T)$ curve at zero field, but becomes visible under 9-T field when T_c is suppressed to lower temperatures, as shown in Figs. 3e and 4e. Upon further increasing pressure, the superconducting transition remains very sharp and T_c moves down slowly to 33.2 K at 8.8 GPa. Due to the large upper critical field, T_m cannot be defined at $P > 6.3$ GPa (Figs. 4f-h). These above findings are further confirmed by separate high-pressure resistivity measurements with a constant-loading CAC, as shown in Fig. 2c.

When the obtained $T_m(P)$ and $T_c(P)$ data are plotted in Fig. 1, we uncover a previously unknown dome-shaped magnetic order with two ends situated near the boundaries separating the three-plateau $T_c(P)$. This observation suggests that the superconductivity in FeSe is intimately correlated with the magnetism. Despite of the absence of static magnetic order within the nematic phase [4–6], strong spin fluctuations with an in-plane wave vector $\mathbf{q} = (\pi, 0)$ have been identified recently [26]. Recent theoretical studies [27] have attributed the absence of static magnetic order to unusual magnetic frustration among multiple competing magnetic orders with $\mathbf{q} = (\pi, \xi)$ with $0 \leq \xi \leq \pi/2$. According to the calculations, this magnetic frustration can be removed under pressure, and gives way to a long-range magnetic order with $\mathbf{q} = (\pi, 0)$. Indeed, the stabilization of static magnetic order at T_m is concomitant with the destruction of nematic order as seen in Fig. 1, thus highlighting the competing nature between nematic and magnetic order. The $\mathbf{q} \neq 0$ nature of the pressure-induced magnetic phase is supported by the Fermi surface reconstruction recently reported from quantum oscillations [19], and also consistent with the field independence of T_m found in the present study (Figs. 4a-e). Thus the pressure-induced order that supersedes the nematic order above ~ 2 GPa is most likely a spin density wave (SDW), although the previous neutron scattering experiment was unsuccessful due to the small magnetic moment [17]. Further studies are needed for the full determination of the detailed magnetic structure of the pressure-induced magnetic phase.

Most importantly, our results reveal unambiguously that the sudden jump of T_c around 6 GPa comes concomitantly with the suppression of magnetic order, demonstrating another competition between the SDW order and high- T_c superconductivity at high pressures. The peak temperature (≈ 45 K) of the $T_m(P)$ dome is quite close to the maximum $T_c (= 38.3$ K), indicating that these competing orders have very similar energy scales. This is different from other iron-based superconductors where the antiferromagnetic transition temperatures in the mother materials are significantly higher than the maximum T_c values of the derived superconducting phases [3, 22]. We note that the non-monotonic dependence of $T_c(P)$ is somewhat akin to the two-dome shape of $T_c(x)$ recently found in $\text{LaFeAsO}_{1-x}\text{H}_x$ [3]. However, the complete dome shape of $T_m(P)$ with two ends in a single phase diagram of FeSe without changing of carrier balance is distinctly different from the $\text{LaFeAsO}_{1-x}\text{H}_x$ case, in which two different antiferromagnetic orders exist near the opposite doping ends of the superconducting phase. Together with the presence of competing nematic order at low pressures, this phase diagram of FeSe thus exhibits unique features among iron-based superconductors. It should be noted that a phase diagram bearing some resemblance has been recently found in hole-doped cuprate superconductors, where the high- T_c superconducting dome is partially suppressed by the presence of dome-shaped charge density wave (CDW) order [2].

It is also intriguing to point out that above the SDW dome, the resistivity curves in the pressure range of ~ 3 -6 GPa show anomalous sub-linear (convex) temperature dependence (Figs. 2b, c), which mimics the suppression of the quasiparticle scattering by the pseudogap formation above the CDW phase of underdoped cuprates. At higher pressures, this convex anomaly in the temperature dependence of resistivity becomes less pronounced. At 8.8 GPa, $\rho(T)$ displays a perfect linear-in- T dependence in a wide temperature range of the normal state (Figs. 2b and 3f), which is a hallmark of non-Fermi-liquid behaviour. The observation of the non-Fermi-liquid behaviour at high pressures where the magnetic order is vanishing is an indication of the presence of strong critical fluctuations. Similar T -linear $\rho(T)$ above T_c has been observed near a quantum critical point (QCP) at $x \approx 0.3$ in the $\text{BaFe}_2(\text{As}_{1-x}\text{P}_x)_2$ system [22]. In that system, the critical fields near the QCP show anomalous features pointing to an enhancement of the energy of superconducting vortices possibly due to a microscopic mixing of antiferromagnetism and superconductivity [28]. This is also supported by the unusually strong vortex pinning found in clean films near the QCP [29]. Our H - T phase diagrams at different pressures indicate that the vortex-liquid region between the

width of transition (T_c and T_c^{peak}) shows a dramatic narrowing when the SDW is suppressed below the superconducting transition (Figs. 4a-h), which can also be accounted for by the enhanced pinning near the QCP. However, a peculiar feature here is that the optimal T_c takes place at the point where T_m just crosses T_c , rather than the possible QCP at $\gtrsim 8$ GPa where T_m completely vanishes. This is again rather similar to the case of hole-doped cuprate superconductors in a sense that a putative QCP is located at the slightly overdoped side [2].

To summarize, by using high pressure as a clean tuning knob, we have clarified in bulk FeSe the interplay of three competing orders, i.e. nematic, magnetic, and superconductivity, and elucidated how the high- T_c superconducting phase is achieved. The relatively low T_c at ambient pressure should be attributed to the presence of competing nematic order; the application of high pressure initially suppresses gradually the nematic order so as to enhance superconductivity. At the same time, the suppression of nematic order also relieves the magnetic frustration so as to stabilize the magnetic order, which then competes again with superconductivity, leading to a local maximum of $T_c(P)$ around 1 GPa. Then, a complete elimination of nematic order around 2 GPa gives rise to a more profound enhancement of T_c to the second plateau of ~ 20 K; the opposite effects on T_c imposed by the strong fluctuations of nematic order and the long-range SDW order produce the local minimum of $T_c(P)$ around 1.5 GPa. Above ~ 2 GPa, only the static SDW order is present and competes with superconductivity so that T_c keeps nearly unchanged while T_m rises until ~ 5 GPa, where the magnetic order at T_m eventually becomes destabilized by pressure. Then, the suppression of magnetic order leads to a great enhancement of T_c to 38 K. In such a way, FeSe exhibits a unique phase diagram with three competing orders, nematic, SDW and high- T_c superconductivity; the latter two of which have very close energy scales. This newly constructed diagram, which shares some similarities to that of cuprates, may offer important clues for discussing the unconventional origins of the high- T_c superconductivity in this class of materials.

METHODS

High-quality FeSe single crystals used in the present study have been grown by two different methods: the chemical vapor transport technique [23] (Kyoto University) and the flux method [30] (Oak Ridge National Laboratory). These two methods yield FeSe single

crystals with similar quality in terms of the phase transition temperatures ($T_s = 87\text{-}90\text{ K}$ and $T_c = 8.5\text{-}9\text{ K}$) and the residual resistivity ratio $\text{RRR} \sim 40$. However, the flux method produces much larger (up to $\sim 10\text{ mm}$) and thicker ($\sim 1\text{ mm}$) crystals and thus we cleaved and cut these samples to fit in the pressure cells. The crystals are well characterized by measuring X-ray diffraction, energy dispersive spectroscopy, magnetic and transport properties under ambient pressure.

High-pressure resistivity $\rho(T, P)$ measurements have been performed under hydrostatic pressures up to $\sim 2\text{ GPa}$ with a piston-cylinder cell (PCC) and up to $\sim 9\text{ GPa}$ with cubic anvil cells (CACs), respectively. For the crystals grown with the flux method, $\rho(T, P, H)$ data under high pressures and magnetic fields were measured in the Institute of Physics, Chinese Academy of Sciences, by using the self-clamped type CAC and PCC. The high-pressure resistivity of crystals grown with the chemical vapor transfer method was measured in the Institute for Solid State Physics, University of Tokyo with a constant-loading type CAC, which can maintain a nearly constant pressure over the whole temperature range from 300 K to 2 K . The pressure value inside the PCC was determined by monitoring the shift of superconducting transition of lead (Pb), while those of CACs were calibrated at room temperature by observing the characteristic transitions of bismuth (Bi). (It should be noted that for the self-clamped pressure cells, both PCC and CAC, the pressure value at room temperature is slightly different from that at low temperature due to the solidification of liquid pressure transmitting medium and the different thermal contraction of cell components. Therefore, some corrections have been made in comparison with the data obtained from the constant-loading CAC). For all these high-pressure resistivity measurements, we employed glycerol as the pressure transmitting medium. All resistivity measurements were performed with the conventional four-terminal method with current applied within the ab plane and magnetic field perpendicular to the ab plane.

ACKNOWLEDGEMENTS

We thank T. Terashima, X. J. Zhou, T. Xiang, R. Yu, Q. M. Zhang, G. Chen, and J.-S. Zhou for very helpful discussions. We also thank Bosen Wang for his technical help. Work at IOP CAS was supported by the National Basic Research Program of China (Grant No. 2014CB921500), National Science Foundation of China (Grant No. 11574377, 11304371),

and the Strategic Priority Research Program of the Chinese Academy of Sciences (Grant No. XDB07020100). Work in Japan was supported by Grant-in-Aids for Scientific Research (A), (B), (S), and on Innovative Areas “Topological Materials Science”. Work at ORNL was supported by the US Department of Energy, Office of Science, Basic Energy Sciences, Materials Sciences and Engineering Division.

- [1] Davis, J. C. S. & Lee, D.-H. Concepts relating magnetic interactions, intertwined electronic orders, and strongly correlated superconductivity. *Proc. Natl. Acad. Sci. USA* **110**, 17623-17630 (2013).
- [2] Keimer, B., Kivelson, S. A., Norman, M. R., Uchida, S., & Zaanen, J. From quantum matter to high-temperature superconductivity in copper oxides. *Nature* **518**, 179-186 (2015).
- [3] Hosono, H. & Kuroki, K. Iron-based superconductors: Current status of materials and pairing mechanism. *Physica C* **514**, 399-422 (2015).
- [4] Imai, T., Ahilan, K., Ning, F. L., McQueen, T. M., & Cava, R. J. Why does undoped FeSe become a high- T_c superconductor under pressure? *Phys. Rev. Lett.* **102**, 177005 (2009).
- [5] Baek, S.-H. *et al.* Orbital-driven nematicity in FeSe. *Nat. Mater.* **14**, 210-214 (2015).
- [6] Böhmer, A. E. *et al.* Origin of the tetragonal-to-orthorhombic phase transition in FeSe: A combined thermodynamic and NMR study of nematicity. *Phys. Rev. Lett.* **114**, 027001 (2015).
- [7] Medvedev, S. *et al.* Electronic and magnetic phase diagram of β -Fe_{1.01}Se with superconductivity at 36.7 K under pressure. *Nat. Mater.* **8**, 630-633 (2009).
- [8] Miyoshi, K. *et al.* Enhanced superconductivity on the tetragonal lattice in FeSe under hydrostatic pressure. *J. Phys. Soc. Jpn.* **83**, 013702 (2014).
- [9] Song, C.-L. *et al.* Direct observation of nodes and twofold symmetry in FeSe superconductor. *Science* **332**, 1410-1413 (2011).
- [10] Kasahara, S. *et al.* Field-induced superconducting phase of FeSe in the BCS-BEC cross-over. *Proc. Natl. Acad. Sci. USA* **111**, 16309-16313 (2014).
- [11] He, S. L. *et al.* Phase diagram and electronic indication of high-temperature superconductivity at 65 K in single-layer FeSe films. *Nat. Mater.* **12**, 605-610 (2013).
- [12] Tan, S. Y. *et al.* Interface-induced superconductivity and strain-dependent spin density wave in FeSe/SrTiO₃ thin films. *Nat. Mater.* **12**, 634-640 (2013).

- [13] Ge, J.-F. *et al.* Superconductivity above 100 K in single-layer FeSe films on doped SrTiO₃. *Nat. Mater.* **14**, 285-289 (2015).
- [14] Miyata, Y., Nakayama, N., Sugawara, K., Sato, T., & Takahashi, T. High-temperature superconductivity in potassium-coated multilayer FeSe thin films. *Nat. Mater.* **14**, 775-779 (2015).
- [15] Shiogai, J., Ito, Y., Mitsuhashi, T., Nojima, T., & Tsukazaki, A. Electric-field-induced superconductivity in electrochemically etched ultrathin FeSe films on SrTiO₃ and MgO. *Nat. Phys.* doi:10.1038/nphys3530 (2015).
- [16] Terashima, T. *et al.* Anomalous Fermi surface in FeSe seen by Shubnikov-de Haas oscillation measurements. *Phys. Rev. B* **90**, 144517 (2014).
- [17] Bendele, M. *et al.* Coexistence of superconductivity and magnetism in FeSe_{1-x} under pressure. *Phys. Rev. B* **85**, 064517 (2012).
- [18] Terashima, T. *et al.* Pressure-induced antiferromagnetic transition and phase diagram in FeSe. *J. Phys. Soc. Jpn.* **84**, 063701 (2015).
- [19] Terashima, T. *et al.* Fermi surface reconstruction in FeSe under high pressure. *arXiv:1510.01840* (2015).
- [20] Kaluarachchi, U.S. *et al.* Non-monotonic pressure evolution of the upper critical field in superconducting FeSe. *arXiv:1511.08766* (2015).
- [21] Jung, S.-G. *et al.* Enhanced critical current density in the pressure-induced magnetic state of the high-temperature superconductor FeSe. *Sci. Rep.* **5**, 16385 (2015).
- [22] Shibauchi, T., Carrington, A., & Matsuda, Y. A quantum critical point lying beneath the superconducting dome in iron-pnictides. *Annu. Rev. Condens. Matter Phys.* **5**, 113-135 (2014).
- [23] Böhmer, A.E. *et al.* Lack of coupling between superconductivity and orthorhombic distortion in stoichiometric single-crystalline FeSe. *Phys. Rev. B* **87**, 180505(R) (2013).
- [24] Matsubayashi, K. *et al.* Pressure-induced heavy fermion superconductivity in the nonmagnetic quadrupolar system PrTi₂Al₂₀. *Phys. Rev. Lett.* **109**, 187004 (2014).
- [25] Cheng, J.-G. *et al.* Integrated-fin gasket for palm cubic-anvil high pressure apparatus. *Rev. Sci. Instrum.* **85**, 093907 (2014).
- [26] Wang, Q. *et al.* Strong interplay between stripe spin fluctuations, nematicity and superconductivity in FeSe. *Nat. Mater.* doi:10.1038/nmat4492 (2015).
- [27] Glasbrenner, J.K. *et al.* Effect of magnetic frustration on nematicity and superconductivity in iron chalcogenides. *Nat. Phys.* **11**, 953-958 (2014).

- [28] Putzke, C. *et al.* Anomalous critical fields in quantum critical superconductors. *Nat. Commun.* **5**, 5679 (2014).
- [29] Kurth, F. *et al.* Unusually high critical current of clean P-doped BaFe₂As₂ single crystalline thin film. *Appl. Phys. Lett.* **106**, 072602 (2015).
- [30] Chareev, D. *et al.* Single crystal growth and characterization of tetragonal FeSe_{1-x} superconductors. *CrystEngComm* **15**, 1989-1993 (2013).

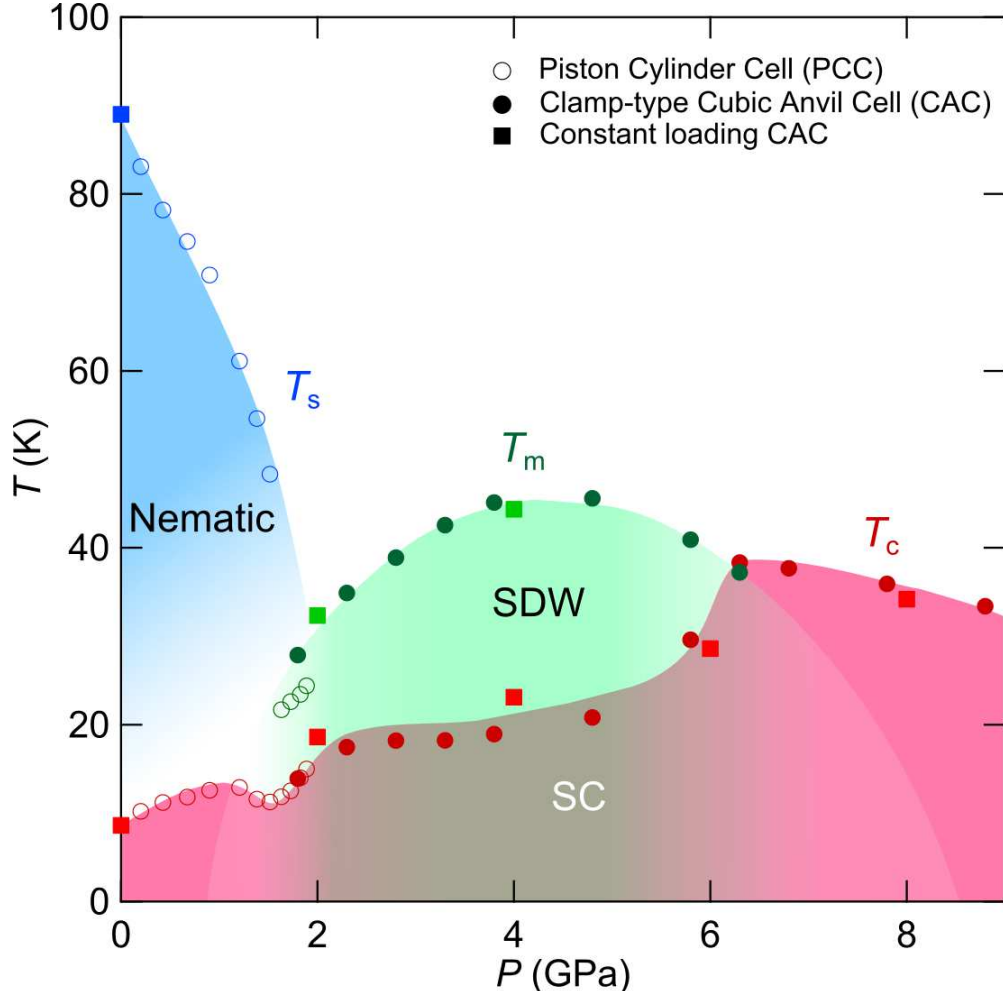


FIG. 1. **Temperature-pressure phase diagram of bulk FeSe.** The structural (T_s , blue), magnetic (T_m , green), and superconducting transition temperatures (T_c , red) as a function of hydrostatic pressure in high-quality single crystals determined by the resistive anomalies measured in the PCC (open circles), clamp-type CAC (closed circles), and constant-loading type CAC (closed squares). The magnetic phase is most likely a spin density wave (SDW) phase. Colour shades for the nematic, SDW, and superconducting (SC) states are guides to the eyes.

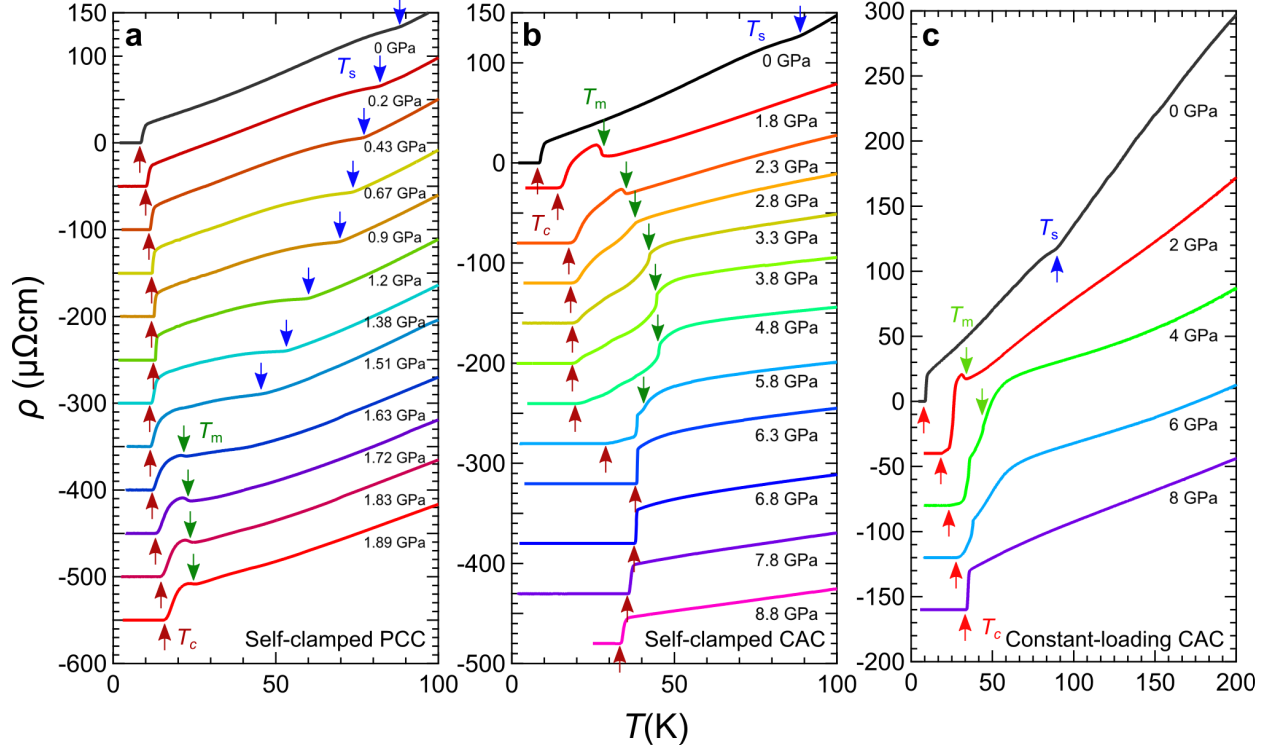


FIG. 2. **Temperature dependence of resistivity in FeSe single crystals under high pressure.** **a**, $\rho(T)$ curves below 100 K at different pressures up to ~ 1.9 GPa measured in the PCC. **b**, Data up to ~ 8.8 GPa measured in the clamp-type CAC. **c**, $\rho(T)$ curves below 200 K up to 8 GPa measured under constant loading forces. For all the plots, the data are vertically shifted for clarity. The resistive anomalies at transition temperatures T_s , T_m , and T_c are indicated by the arrows.

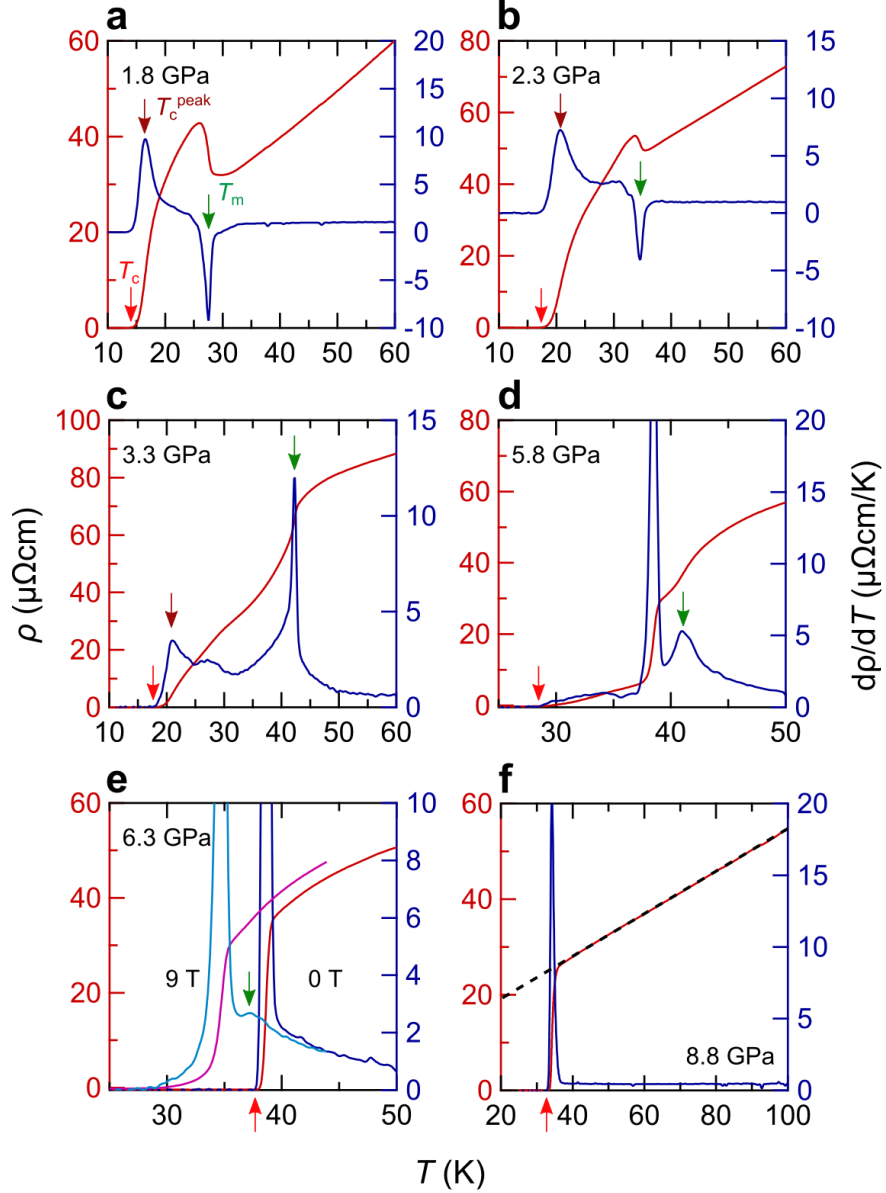


FIG. 3. **Determination of magnetic and superconducting transition temperatures from the resistivity curves under high pressure.** a-f, Temperature dependence of resistivity $\rho(T)$ (left axis) and temperature derivative of resistivity $d\rho/dT(T)$ (right axis) at low temperatures. The temperature at the maximum slope of superconducting transition is defined as T_c^{peak} and the zero resistivity temperature as T_c . The magnetic transition temperature T_m is determined by the dip or peak in $d\rho/dT(T)$. At 6.3 GPa, the data at 9 T is also shown where T_m anomaly appears when the superconducting transition is shifted down (e). At 8.8 GPa, the normal-state resistivity can be fitted to a T -linear dependence (dashed line in f).

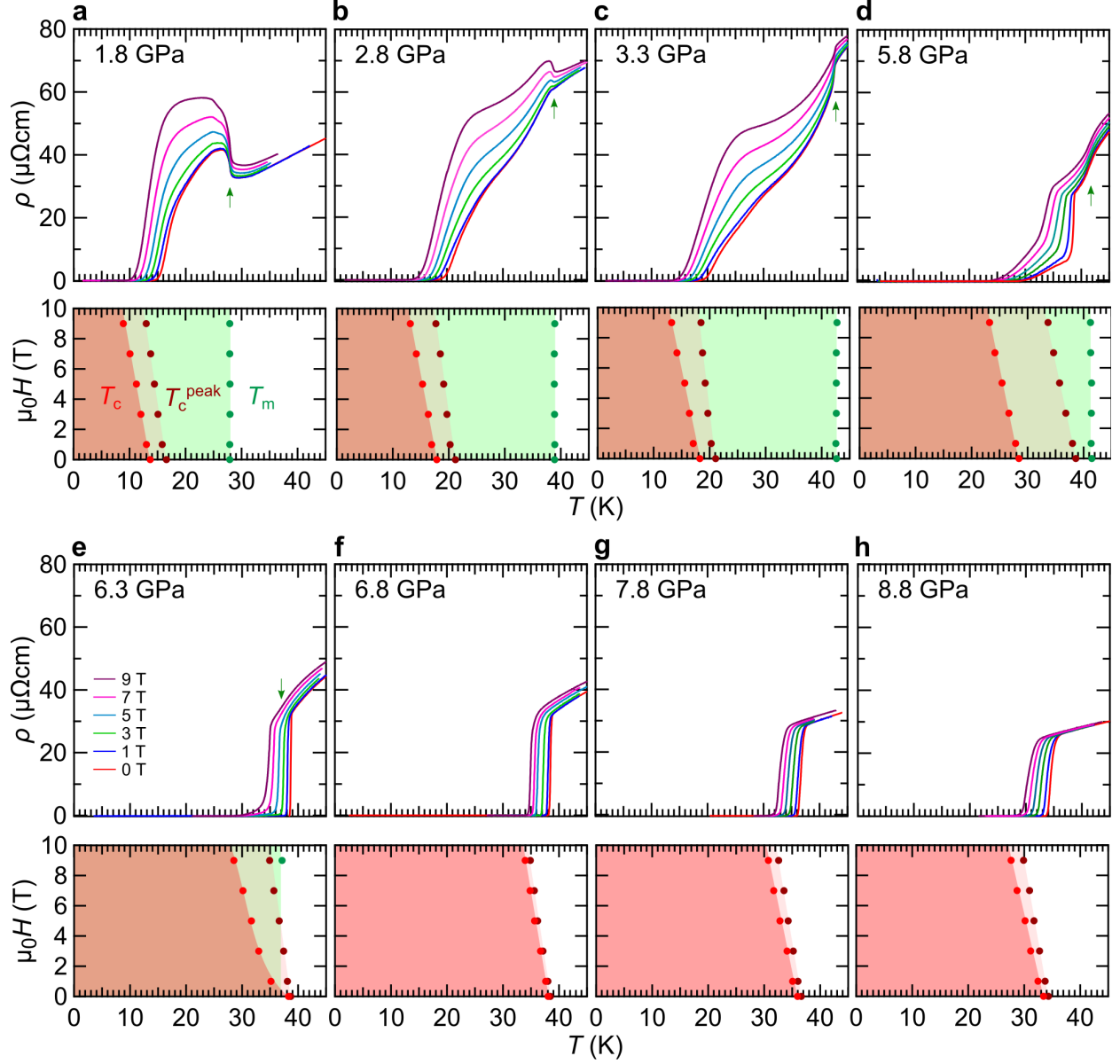


FIG. 4. **Effects of magnetic fields on the magnetic and superconducting transitions under high pressure.** **a-h**, Upper panels show $\rho(T)$ curves at different magnetic fields applied parallel to the c axis. The antiferromagnetic transition temperature T_m is field independent and marked by the green arrow (**a-d**). At 6.3 GPa, the T_m anomaly is only visible at high fields (**e**). Lower panels show H - T phase diagrams. The zero resistivity is attained below T_c and the T_c^{peak} line (see the definition in Fig. 3a) is a lower bound of upper critical field H_{c2} . The sharp superconducting transitions under magnetic fields for $P > 6.3$ GPa indicate narrowed regimes of the vortex liquid state.